International Journal of Quantum Information
Vol. 15, No. 8 (2017) 1740021 (10 pages)

DOI: 10.1142/S0219749917400214

World Scientific
www.worldscientific.com

Generation of quasi-single-mode twin-beam states in the high-intensity domain

Alessia Allevi*,†,‡, Giovanni Chesi*,§ and Maria Bondani†,¶

*Department of Science and High Technology,
University of Insubria,
Via Valleggio 11, I-22100 Como, Italy

†Institute for Photonics and Nanotechnologies, IFN-CNR,
Via Valleggio 11, I-22100 Como, Italy
‡alessia.allevi@uninsubria.it
§gchesi@uninsubria.it
¶maria.bondani@uninsubria.it

Received 22 September 2017
Accepted 1 December 2017
Published 22 December 2017

Single-mode quantum optical states represent an interesting resource for the implementation of quantum information protocols. Here, we address the generation of twin-beam (TWB) states characterized by a quasi-single-mode thermal statistics. In more detail, the selection procedure leading to single-mode states is achieved with a strong filtering applied to intense TWBs generated in a single crystal by parametric downconversion. We investigate the role of pump power in the production of the single-mode states and compare the results obtained with nonlinear crystals having different lengths.

Keywords: Quantum optics; parametric downconversion; photodetectors.

1. Introduction

Quantum optical states endowed with sizeable numbers of photons in each pulse represent a desirable resource for the implementation of quantum information protocols since they are more robust with respect to losses than single-photon states. Indeed, losses can be considered as the only form of decoherence affecting optical systems. However, till now, the exploitation of such states has been limited because of two main reasons, namely the optimization of their generation and the efficiency of their detection. Regarding the former aspect, the production of quantum states of light relies on the realization of nonlinear processes, such as the well-known process of spontaneous parametric downconversion (PDC). As already demonstrated in many experimental works performed at different intensity regimes, the twin-beam

‡Corresponding author.

(TWB) states generated by the PDC process exhibit sub-shot-noise, i.e. nonclassical, photon-number correlations between the two parties.[1–7] Thanks to this feature, TWBs represent a useful resource for the development of quantum technologies, ranging from quantum imaging[8–13] and wide-field microscopy[14] to quantum metrology.[15] A key role in some of these applications is played by the multi-mode nature of TWBs, to which the finite spatial and spectral profile of the pump and the possibility to generate light even in phase-mismatch conditions contribute.[16–18]

Even if the multi-mode nature, which reflects in the statistical properties of the generated light,[19] is natural, its description is quite difficult. In fact, the theoretical description of the TWB state generated by the PDC process is single mode.[20] On the one hand, such an assumption simplifies the calculations, on the other hand, there are quantities, such as the quantum discord,[21] which are well defined if and only if the states contain a single mode. Moreover, for what concerns the possible applications, there are situations in which the single-mode nature is not desirable, but strongly required, such as to overcome Gaussian no-go theorems,[22] to enable continuous-variable entanglement distillation[23,24] and to allow for the preparation of cat states.[25,26]

Till now, the generation of single-mode TWB states has been achieved by means of waveguide systems, which act as spatial and spectral mode selectors.[7,27,28]

In this paper, we address the generation of quasi-single-mode states by sending the TWB states generated in a bulky material to an imaging spectrometer and collecting a small portion of the output field by means of a multi-mode fiber connected to a hybrid photodetector (HPD). In particular, we study the conditions of pump power and crystal length that enable the achievement of a quasi-single-mode state.

2. Theory

The Hamiltonian of a multi-mode PDC process can be expressed as follows:

$$\hat{H} = \sum_{j}^{\mu} \hat{H}_j, \tag{1}$$

in which μ is the number of independent contributions

$$\hat{H}_j \propto \hat{a}^{\dagger}_{\mathrm{si},j} \hat{a}^{\dagger}_{\mathrm{id},j} \hat{a}_{\mathrm{pu}} + \mathrm{h.c.}, \tag{2}$$

each coupling three monochromatic field modes: pump (pu), signal (si) and idler (id), identified by their frequencies and wavevectors. $\hat{a}^{\dagger}_{l,j}$ are the field-mode operators satisfying the commutation rules $[\hat{a}_{l,j}, \hat{a}^{\dagger}_{l,i}] = \delta_{j,i}$ for $l = \mathrm{si}, \mathrm{id}$.

In the so-called parametric approximation, that is by neglecting the evolution of the pump field during the interaction, and by assuming that the process starts from the vacuum, the generated state can be written as[29]

$$|\psi_{\mu}\rangle = \sum_{n=0}^{\infty} \sqrt{P(n)} |n^{\otimes}\rangle |n^{\otimes}\rangle, \tag{3}$$

where $|n^{\otimes}\rangle = \delta(n - \sum_{h=1}^{\mu} n_h) \bigotimes_{k=1}^{\mu} |n\rangle_k$ represents the overall n photons coming from the μ modes that impinge on the detector and $P(n)$ is the multi-mode thermal distribution

$$P(n) = \frac{(n+\mu-1)!}{n!(\mu-1)!(\langle n\rangle/\mu+1)^{\mu}(\mu/\langle n\rangle+1)^{n}}, \tag{4}$$

in which $\langle n\rangle/\mu$ is the mean number of photons per mode.

The multi-mode nature of TWB emerging from Eq. (3) can be explained according to two possible approaches. In the first scenario, the pump beam is treated as a plane-wave undepleted field, whereas in the second one, it is allowed to evolve together with signal and idler fields. Concerning the first model, as already explained in Refs. 13, 16 and 30, the frequency- and phase-matching conditions allow the generation of TWBs on a continuum of frequencies and propagation directions linked to each other by nontrivial relations. Moreover, the possibility to generate light in conditions of phase-mismatch produces an output field characterized by the simultaneous presence of many modes, both spatial and temporal. As to the spatial modes, the far-field single-shot images of the output field display a "speckle" pattern, which can be interpreted as follows: the center of each speckle individuates the direction of one of the phase-matched wavevectors, whereas the size of the speckle depends on the angular bandwidth allowed by phase mismatch. As to the temporal modes, in the case of a pulsed field, they can be viewed as the ratio of the temporal bandwidth of the nonlinear process to the spectral bandwidth of the pump field. The presence of temporal modes reflects on the photon-number statistics of the light inside a single spatial mode.

This description is particularly useful to describe low-intensity TWBs in the parametric approximation. However, also in the high-gain regime, the pump field evolves and thus the system becomes more complex. In this case, the best description of the PDC output is given in terms of Schmidt modes.

At the single-photon level, this approach is extensively used and gives the biphoton function, which is expressed as a sum of factorized terms[31]:

$$|\psi\rangle = \sum_k \lambda_k |u_k\rangle |v_k\rangle. \tag{5}$$

Here, $|u_k\rangle$ and $|v_k\rangle$ represent the eigenvectors of the orthonormal dual basis of the Schmidt modes, whereas the eigenvalues λ_k give the probabilities p_k of detecting a photon in kth mode, namely $p_k = \lambda_k^2$. In this representation, the multi-mode nature of the TWB is expressed by the Schmidt number

$$K = \frac{1}{\sum_k \lambda_k^4}, \tag{6}$$

which is also connected in a simple way to the second-order autocorrelation function g^2:

$$g^2 = \frac{\langle : \hat{n}_l^{\,2} : \rangle}{\langle n_l \rangle^2} = 1 + \frac{1}{K}, \tag{7}$$

where : · · : refers to normal ordering and $\langle n_l \rangle$ is the mean number of photons either in the signal or in the idler arm. Note that the Schmidt number K coincides with the number of modes μ of the photon-number statistics.

In contrast to low-gain PDC, developing a consistent theoretical description of high-gain TWBs is a difficult problem due to the contribution of correlated high-order Fock components and therefore due to the nonapplicability of a perturbation theory. As already demonstrated in Refs. 32 and 33, a way to approach the Schmidt decomposition of high-gain TWB is to define polychromatic modes that allow a formally similar description as in the low gain regime. According to this model, Eq. (7) holds also for intense TWBs.

3. Experiment

3.1. *Experimental setup*

In order to investigate the experimental conditions under which a single spatio-spectral mode can be selected, we generated intense TWB states by sending the third harmonic pulses at 349 nm of a Nd:YLF laser regeneratively amplified at 500 Hz to a type-I β-Barium borate (BBO) crystal. As shown in Fig. 1, the pump size was set to 250 μm by means of a telescope placed in front of the crystal, whereas the pump power was changed by means of a half-wave plate, followed by a polarizing cube beam splitter located in front of the telescope. As to the nonlinear medium, during our investigation, we used some BBO crystals having different lengths (2, 3, 4, 6 and 15 mm). In each case, the crystal was tuned to have the phase-matching condition at frequency degeneracy in quasi-collinear configuration (33.8°). After the removal of the pump beam by means of a mirror and an edge filter, the broadband PDC light was collected by a 100-mm-focal-length lens and focused on the plane of the vertical slit of an imaging spectrometer (SR-303i-B, mod. Shamrock, Andor) having a 1200-line/mm grating inside. Thanks to its structure, this device is used to make a 1:1 imaging of the slit plane on the exit plane. The presence of the grating gives access to the investigation of the spectral features of the input light together with the spatial ones. The typical speckle-like pattern that can be observed at the output plane with a synchronized camera is shown in Fig. 2. The existence of intensity correlations between the signal and idler portions of the TWB is supported by the presence of

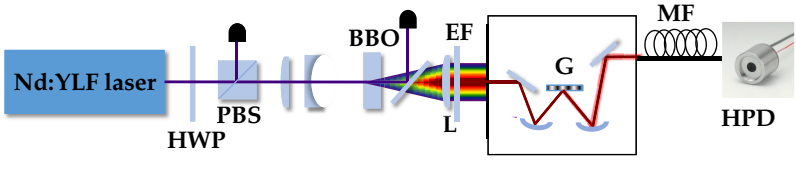

Fig. 1. Sketch of the experimental setup: HWP: half-wave plate; PBS: polarizing cube beam splitter; BBO: β-Barium borate crystal; L: 100-mm-focal-length lens; EF: edge filter; G: grating; MF: multi-mode fiber; HPD: hybrid photodetector.

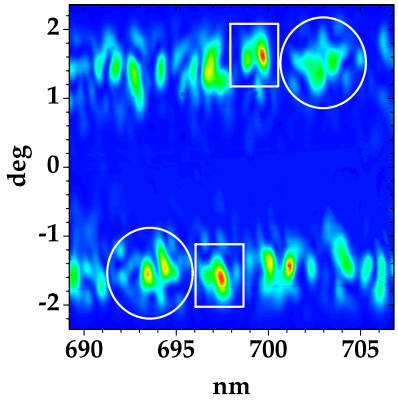

Fig. 2. Single-shot image recorded by a synchronized camera, in which the typical speckle-like pattern of PDC in the spatio-spectral domain is clearly evident. The horizontal axis refers to spectrum, whereas the vertical axis to the angular dispersion. In the figure, the full-spectral bandwidth is 17.6 nm wide, whereas the full-angular bandwidth is 4.71° large.

symmetrical structures (actually, they are spatio-spectral coherence areas) around the degenerate wavelength and the collinear direction.[32]

A 300-μm-core diameter multi-mode fiber was located instead of the camera at the exit plane of the device in order to roughly collect a single spatio-spectral area in one arm of the TWB. Note that, in principle, a second fiber can be used to simultaneously collect the light coming from the correlated spatio-spectral area. This procedure is essential, for instance, to study the strength of the photon-number correlations between the two parties of the TWB state. However, as in this work we are mainly interested in investigating the parameters useful to tailor the number of spatio-spectral modes, we focus our attention only on one single arm.

The multi-mode fiber was mounted on a three-axis translation stage. The light was then delivered to an HPD (mod. R10467U-40, Hamamatsu, nominal quantum efficiency 30% at 698 nm), whose output was amplified (preamplifier A250 plus amplifier A275, Amptek), synchronously integrated (SGI, SR250, Stanford), and digitized (ADC, PCI-6251, National Instruments). The HPD is a commercial photon-number-resolving detector composed of a photocathode followed by an avalanche diode operated below the breakdown threshold. According to the model already presented in Refs. 13 and 34, the detection process consists of two steps: photo-detection by the photocathode and amplification. The first process is described by a Bernoullian convolution, whereas the second one can be approximated by the multiplication by a constant gain factor. We have already demonstrated that the value of the gain can be obtained by means of a self-consistent method[34] based on the very light to be measured. Once the value of the gain is determined, we have direct access to the shot-by-shot number of detected photons and we can thus evaluate the statistical properties of the measured states. To this aim, all the results presented in the following were obtained by acquiring sequences of 100,000 single shots for different

intensity values of the pump beam. A set of neutral-density filters was used to suitably attenuate the light and keep it within the detector dynamics.

3.2. *Experimental results*

In Fig. 3, we show the reconstruction of two detected-photon distributions obtained by using a 4-mm-long BBO crystal as the nonlinear medium for two different choices of pump power. As already explained in Sec. 3.1, we used neutral-density filters to keep the values of the light within the dynamic range of the HPD detector. For this reason, there is no direct connection between the pump power values and the measured mean values of the TWB. Since the light measured on either signal or idler separately is classical, the presence of the filters does not change the photon-number distribution, which is described by Eq. (4) and does not affect the number of independent modes μ.[35] The experimental data (gray columns + black error bars) are shown in the figure together with the multi-mode thermal fitting curves (red dots) obtained according to Eq. (4), in which the mean value $\langle m \rangle$ is fixed to the values experimentally measured and the number of modes, μ, is the only fitting parameter.

The number of modes can be also obtained by considering only the first two moments of the photon-number statistics. In particular, it can be obtained from

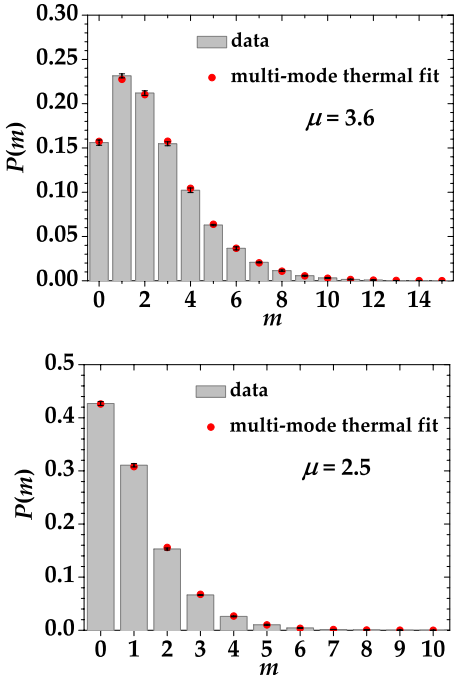

Fig. 3. (Color online) Experimental detected-photon number distributions (gray columns + black error bars), and multi-mode thermal fitting functions (red dots) for two different choices of pump power values (upper panel: $P_{UV} = 133.5\,mW$, lower panel: $P_{UV} = 87\,mW$). The good agreement between the data and the theoretical expectation is testified by the high values of fidelity (more than 99.99% in both panels).

Eq. (7), suitably rewritten in terms of detected photons. By considering the relation between the autocorrelation function g^2 and the analogous quantity for detected photons[36]

$$g_m^2 = \frac{\langle m^2 \rangle}{\langle m \rangle^2} = g^2 + \frac{1}{\langle m \rangle}, \tag{8}$$

where $\langle m \rangle$ is the mean number of detected photons, the number of modes can be expressed as

$$\mu = \frac{\langle m \rangle^2}{\sigma^2(m) - \langle m \rangle}, \tag{9}$$

in which $\sigma^2(m)$ is the variance of the distribution.

By using this relation, we calculated the number of modes at different pump power values for each choice of BBO crystal. For a direct comparison, in Fig. 4, we show the experimental values of μ for four different choices of crystals, namely 2-, 3-, 4- and 6-mm-long ones. It appears evident that for 3-, 4- and 6-mm-long BBO crystals, the number of modes is evolving. In particular, at low pump powers, the values of μ start decreasing, reach a minimum and then increase again. As already explained in Refs. 32 and 33, such a behavior can be explained by admitting that at high-gain values, not only the signal and idler fields evolve, but also the pump field, and thus the dynamics of the system becomes more complex. By assuming that the number of effectively populated signal and idler radiation modes depends on the pump power, when the pump power increases, the PDC gain profile becomes narrower and narrower and thus the signal and idler fields are dominantly emitted into a smaller and smaller number of modes that gain energy to the detriment of the others.[37,38] For sufficiently high values of the pump power, the process of mode selection reverts as the pump profile undergoes depletion. For this reason, the gain of the high-populated lower-order modes is reduced, whereas the gain of low-populated higher-order modes

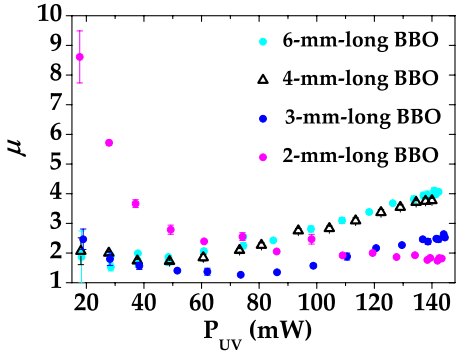

Fig. 4. (Color online) Number of modes μ as a function of pump power values P_{UV} for different BBO crystals. Magenta dots: 2-mm-long BBO; blue dots: 3-mm-long BBO; black triangles: 4-mm-long BBO; cyan dots: 6-mm-long BBO. In all cases, the light was collected by means of a 300-μm-core-diameter multi-mode fiber.

is supported. In the case of the 2-mm-long crystal, the short length of the medium prevents the observation of the entire evolution. On the contrary, a sort of plateau is reached at high pump power values. Moreover, by comparing the pump power values at which the minimum number of modes is reached, we also note that the longer the crystal, the faster the evolution. However, it is hard to find a clear dependence of the position of this minimum on the length of the crystal because of the complexity of the system. It is also remarkable that the absolute values of μ are not the same for all the crystals. On the contrary, it seems that the shorter the crystal, the smaller the values of μ that can be achieved. However, for none of the crystals, the employed configuration allowed the selection of a single spatio-spectral mode. Therefore, we decided to repeat the measurements by using a narrower fiber, that is with a 100-μm-core-diameter fiber instead of the 300-μm-core-diameter one.

For a fair comparison, in Fig. 5, we show the number of modes as a function of the pump power in the case of the 4-mm-long crystal, which represents a good compromise, with the two choices of fiber diameters. We can immediately note that the narrower the fiber, the lower the number of modes. Moreover, the choice of the fiber does not affect the evolution of μ at different pump power values. For instance, the minimum value of μ occurs at the same pump power value in both the cases.

By repeating the measurements with the 100-μm-core-diameter fiber, we were thus able to select a quasi-single spatio-spectral mode in all cases. The experimental results are shown in Fig. 6 as colored symbols. With this configuration, we decided not to use the 2-mm-long crystal as the amount of light collected by the fiber was small. On the contrary, we decided to exploit a very long crystal, that is the 15-mm-long one. By comparing the different BBO crystals, we can recognize that the longer the crystal, the faster the evolution of μ and in particular, the achievement of the minimum value. At the same time, we remark that the shorter the medium, the smaller the minimum number of modes that can be achieved. According to these observations, the best choice for the selection of a single mode is provided by the 3-mm-long BBO

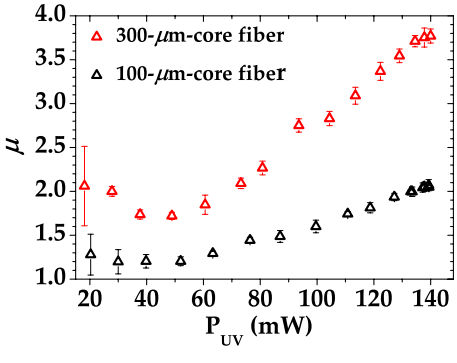

Fig. 5. (Color online) Number of modes μ as a function of pump power values P_{UV} for the 4-mm-long BBO crystal and different multi-mode fibers. Black triangles: 100-μm-core-diameter multi-mode fiber; red triangles: 300-μm-core-diameter multi-mode fiber.

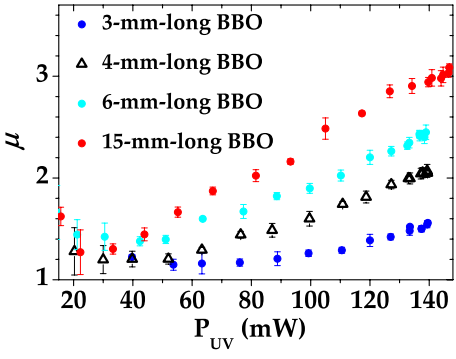

Fig. 6. (Color online) Number of modes μ as a function of pump power values P_{UV} for different BBO crystals. Blue dots: 3-mm-long BBO; black triangles: 4-mm-long BBO; cyan dots: 6-mm-long BBO; red dots: 15-mm-long BBO. In all cases, the light was collected by means of a 100-μm-core-diameter multi-mode fiber.

crystal, for which we have $\mu = 1.15$. We also note that, at variance with longer crystals, its behavior is smoother and thus the evolution of the generated light is less dependent on pump power values.

4. Conclusions

In conclusion, by using a traveling-wave interaction geometry, we generated intense TWBs and applied a spatio-spectral filtering to them in order to obtain quasi-single-mode optical states. To achieve this result, we exploited an imaging spectrometer at whose output we placed a multi-mode fiber having a core diameter of 100 μm. We showed that, besides the selection procedure offered by the employed instrumentation, the pump field also plays a crucial role in the achievement of the single-mode condition. In particular, the progressive occurrence of pump depletion decreases the number of modes describing the PDC field as well as the number of statistical modes. We also investigated the role of the crystal length by comparing different BBO crystals. Even if it is hard to find an exact relation, from the comparison among the crystals, it is quite evident the way in which the number of modes depends on the length of the nonlinear medium. Indeed, it is remarkable that the investigations of all the parameters characterizing the system under examination represent a key step towards its thorough understanding.

Acknowledgment

We thank Prof. Ondřej Haderka for loaning the imaging spectrometer.

References

1. O. Jedrkiewicz *et al.*, *Phys. Rev. Lett.* **93** (2004) 243601.
2. M. Bondani *et al.*, *Phys. Rev. A* **76** (2007) 013833.

3. I. N. Agafonov *et al.*, *Phys. Rev. A* **82** (2010) 011801.
4. G. Brida *et al.*, *Phys. Rev. Lett.* **102** (2009) 213602.
5. D. A. Kalashnikov *et al.*, *Opt. Lett.* **37** (2012) 2829.
6. M. Lamperti *et al.*, *J. Opt. Soc. Am. B* **31** (2014) 20.
7. G. Harder *et al.*, *Phys. Rev. Lett.* **116** (2011) 143601.
8. A. Mosset *et al.*, *Phys. Rev. Lett.* **94** (2005) 223603.
9. E. Brambilla *et al.*, *Phys. Rev. A* **77** (2008) 053807.
10. G. Brida *et al.*, *Nat. Photonics* **4** (2010) 227.
11. M. Genovese, *J. Opt.* **18** (2016) 073002.
12. A. Allevi and M. Bondani, *J. Opt.* **19** (2017) 064001.
13. A. Allevi and M. Bondani, *Adv. At. Mol. Opt. Phys.* **66** (2017) 49.
14. N. Samantaray *et al.*, *Light Sci. Appl.* **6** (2017) e17005.
15. A. Meda *et al.*, *J. Opt.* **19** (2017) 094002.
16. M. Bondani *et al.*, *Eur. Phys. J. Spec. Top.* **203** (2012) 151.
17. G. Brida *et al.*, *Int. J. Quantum Inform.* **7** (2009) 139.
18. G. Brida *et al.*, *J. Mod. Opt.* **56** (2009) 201.
19. F. Paleari *et al.*, *Opt. Express* **12** (2004) 2816.
20. L. Mandel and E. Wolf, *Optical Coherence and Quantum Optics* (Cambrige University Press, New York, 1995).
21. P. Giorda and M. G. A. Paris, *Phys. Rev. Lett.* **105** (2010) 020503.
22. J. Eisert *et al.*, *Phys. Rev. Lett.* **89** (2002) 137903.
23. H. Takahashi *et al.*, *Nat. Photonics* **4** (2010) 178.
24. Y. Kurochkin *et al.*, *Phys. Rev. Lett.* **112** (2014) 070402.
25. A. Ourjoumtsev *et al.*, *Nature* **448** (2007) 784.
26. T. Gerrits *et al.*, *Phys. Rev. A* **82** (2010) 031802.
27. W. P. Grice *et al.*, *Phys. Rev. A* **64** (2001) 063815.
28. A. Eckstein *et al.*, *Phys. Rev. Lett.* **106** (2011) 013603.
29. A. Allevi *et al.*, *Phys. Rev. A* **85** (2012) 063835.
30. A. Gatti *et al.*, *Int. J. Quantum Inform.* **12** (2014) 1461016.
31. A. Christ *et al.*, *New J. Phys.* **13** (2011) 033027.
32. A. Allevi *et al.*, *Phys. Rev. A* **90** (2014) 063812.
33. J. Peřina *et al.*, *Sci. Rep.* **6** (2016) 22320.
34. M. Bondani *et al.*, *J. Mod. Opt.* **56** (2009) 226.
35. A. Allevi and M. Bondani, *J. Opt. Soc. Am. B* **31** (2014) B14.
36. A. Allevi and M. Bondani, *Sci. Rep.* **7** (2017) 16787.
37. W. Wasilewski *et al.*, *Phys. Rev. A* **73** (2006) 063819.
38. A. M. Perez *et al.*, *Opt. Lett.* **39** (2014) 2403.